

PAPER • OPEN ACCESS

EEGdenoiseNet: a benchmark dataset for deep learning solutions of EEG denoising

To cite this article: Haoming Zhang *et al* 2021 *J. Neural Eng.* **18** 056057

View the [article online](#) for updates and enhancements.

You may also like

- [Reference layer adaptive filtering \(RLAF\) for EEG artifact reduction in simultaneous EEG-fMRI](#)
David Steyrl, Gunther Krausz, Karl Koschutnig et al.
- [A simple method for EEG guided transcranial electrical stimulation without models](#)
Andrea Cancelli, Carlo Cottone, Franca Tecchio et al.
- [A new automated multi-stage system of non-local means and multi-kernel adaptive filtering techniques for EEG noise and artifacts suppression](#)
Ahmed S Eltrass and Noha H Ghanem



PAPER

EEGdenoiseNet: a benchmark dataset for deep learning solutions of EEG denoising

OPEN ACCESS

RECEIVED
3 April 2021REVISED
24 September 2021ACCEPTED FOR PUBLICATION
29 September 2021PUBLISHED
14 October 2021

Original Content from
this work may be used
under the terms of the
[Creative Commons
Attribution 4.0 licence](#).

Any further distribution
of this work must
maintain attribution to
the author(s) and the title
of the work, journal
citation and DOI.

Haoming Zhang^{1,4} , Mingqi Zhao^{1,2,4} , Chen Wei¹ , Dante Mantini^{2,3} , Zherui Li¹
and Quanying Liu^{1,*} ¹ Shenzhen Key Laboratory of Smart Healthcare Engineering, Department of Biomedical Engineering, Southern University of Science and Technology, Shenzhen 518055, People's Republic of China² Movement Control and Neuroplasticity Research Group, KU Leuven, Leuven 3001, Belgium³ Brain Imaging and Neural Dynamics Research Group, IRCCS San Camillo Hospital, Venice 30126, Italy⁴ Equal contribution.

* Author to whom any correspondence should be addressed.

E-mail: liuqy@sustech.edu.cn**Keywords:** deep learning, neural network, EEG dataset, benchmark dataset, EEG artifact removal, EEG denoisingSupplementary material for this article is available [online](#)**Abstract**

Objective. Deep learning (DL) networks are increasingly attracting attention across various fields, including electroencephalography (EEG) signal processing. These models provide comparable performance to that of traditional techniques. At present, however, there is a lack of well-structured and standardized datasets with specific benchmark limit the development of DL solutions for EEG denoising. **Approach.** Here, we present EEGdenoiseNet, a benchmark EEG dataset that is suited for training and testing DL-based denoising models, as well as for performance comparisons across models. EEGdenoiseNet contains 4514 clean EEG segments, 3400 ocular artifact segments and 5598 muscular artifact segments, allowing users to synthesize contaminated EEG segments with the ground-truth clean EEG. **Main results.** We used EEGdenoiseNet to evaluate denoising performance of four classical networks (a fully-connected network, a simple and a complex convolution network, and a recurrent neural network). Our results suggested that DL methods have great potential for EEG denoising even under high noise contamination. **Significance.** Through EEGdenoiseNet, we hope to accelerate the development of the emerging field of DL-based EEG denoising. The dataset and code are available at <https://github.com/nclabstustech/EEGdenoiseNet>.

1. Introduction

Electroencephalography (EEG) solutions permit recording of changes in electrical potential on the scalp, which are generated by neurons in the gray matter. EEG is one of the most important direct and non-invasive approaches for studying brain activity under task and resting conditions. It has been widely used in psychology, neurology and psychiatry research, as well as for brain-computer interface [1–6].

EEG signals contain not only brain activity, but also a variety of noise and artifacts, including ocular [7], myogenic artifacts [8, 9], and, in rare cases, cardiac artifacts. Therefore, a basic step in using EEG data to study neural activity is denoising or artifact attenuation [10]. Ocular and myogenic artifacts contaminate EEG signals in different ways. The

former is often visible as relatively large pulses in the frontal region [11], while the latter frequently appears in the temporal and occipital regions, and has a wide frequency spectrum [9, 12].

Various traditional denoising techniques have been developed to remove artifacts from EEG data, such as regression-based methods, adaptive filter-based methods and blind source separation (BSS)-based methods. Among them, the regression-based method first obtains the noise signal through the noise template, and then subtracts the estimated noise signal from the EEG data to eliminate the artifacts [12–15]. On the contrary, methods based on adaptive filters rely on dynamically estimating filter coefficients based on the input EEG signal itself, thereby filtering out noise [16, 17]. BSS-based methods decompose the EEG signal

into multiple components [18–20], assign them to neural and artifactual sources, and reconstruct a clean signal by recombining the neural components [9, 12, 21]. However, BSS-based methods can only be used when a large number of electrodes are available, which are not suitable for single-channel denoising.

Deep learning (DL) have been increasingly attracting attention in the past few years [22–25]. Due to the increase in computing resources, the boosting data size, and the availability of new network architectures and learning algorithms, the performance of DL neural networks has made great breakthroughs, and DL has been successfully applied to solve various technical problems, such as image processing [22, 23, 26, 27] and natural language processing [24, 25, 28]. DL methods have begun to be introduced into the field of EEG signal analysis [29], such as EEG-based classification [30–32], EEG reconstruction [33, 34] and EEG signal generation [35, 36]. Recently, DL has also been applied to EEG denoising, providing performance comparable to the traditional denoising method [37–40].

Deep neural networks can learn the hidden state of neural oscillations in EEG, thereby eliminating fluctuations that are not from real neural activity but from biological artifacts. The performance of deep neural networks fundamentally depends on the size of the training and test datasets; or in other words, it requires big data [41–43]. A big dataset with the gold standard clean EEG is essential for evaluating newly developed supervised DL models. Some EEG datasets have been collected while participants are at rest [44, 45], during cognitive tasks [46–48], or motor-related tasks [49–52]. However, none of them are specifically developed for training end-to-end DL models for EEG artifact removal. To the best of our knowledge, there is no open EEG dataset suitable for training DL models for EEG denoising. The lack of ground-truth clean EEG data and benchmarks have largely limited the development of DL methods for EEG denoising.

In this study, we present a publicly available structured dataset, named EEGdenoiseNet, which is particularly suitable for deep network-based EEG artifacts attenuation (section 2). Specifically, the dataset contains 4514 clean EEG segments as ground truth, and 3400 pure electrooculography (EOG) segments and 5598 pure electromyography (EMG) segments as ocular artifacts and myogenic artifacts respectively. In addition, we also implement four deep neural networks as benchmarks (section 3), including a fully-connected neural network (FCNN), a simple convolution neural network (CNN), a complex CNN, and a recurrent neural network (RNN). We train the DL models in a supervised end-to-end fashion, and the denoising performance are presented as benchmarks (section 4).

2. EEGdenoiseNet dataset

2.1. Data acquisition and preprocessing

Our main goal is to construct a dataset suitable for EEG denoising research based on DL networks. In this regard, we downloaded EEG, EOG and EMG data from several publicly available data repositories which were published in previous studies (see table 1) [53–60]. These studies have been ethically approved by their respective local ethical committees, and followed the Helsinki Declaration of 1975, revised in 2000.

To generate clean EEG, pure EOG and pure EMG, we firstly preprocessed the data. Then segmented them into 2 s segments. Afterwards, we re-scaled the segments to the same variance. Finally, each segment was visually checked by an expert to ensure they are clean and usable. We set the length of segments to 2 s according to the previous knowledge of EEG signals. On the one hand, a 2 s segment is long enough to recover the temporal and spectral characteristics of EEG, as well as EOG and EMG. On the other hand, it is difficult to obtain artifact-free EEG segments longer than 2 s due to the random eye blinks or movements. The segments in each category have been uploaded to a publicly available repository (<https://github.com/nclabstus-tech/EEGdenoiseNet>).

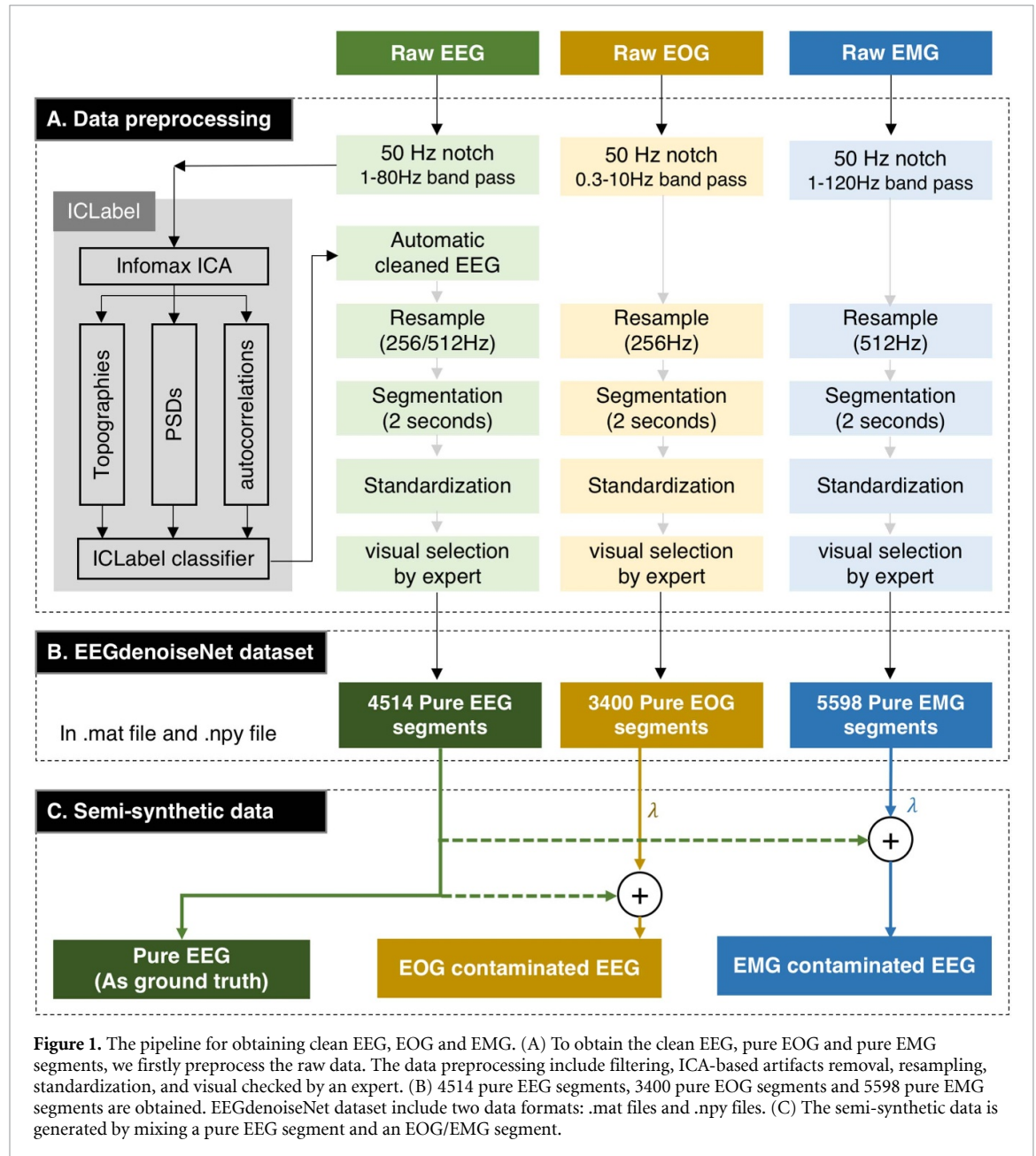
Specifically, for the EEG segments (figure 1(a)) [53], the dataset included 52 participants who performed both real and imaginary left and right hand movement task, with 64 channel EEG recorded simultaneously at 512 Hz sampling frequency. For both real and imagined movement task, a participant repeated 2 s baseline and 3 s movement with 4.1–4.8 s random interval for 20 min. The data was band-pass filtered between 1 and 80 Hz, notched at powerline frequency, and then re-sampled to 256 Hz. To obtain the clean EEG as ground truth, the 64-channel EEG signals were processed by ICLabel, a toolbox to remove EEG artifacts with independent component composition (ICA) [9]. Then the pure EEG signals were segmented into one-dimensional segments of 2 s. It is worth noting that, in order to ensure the universality of this data set, we did not construct clean EEG signals with a specific number of channels due to the diversity of EEG caps, but constructed a dataset with single-channel EEG signal.

For the ocular artifact segments (figure 1(b)), multiple open-access EEG datasets with additional EOG channels are used [54–58,60]. The horizontal and vertical raw EOG signals of the datasets are band-pass filtered between 0.3 and 10 Hz, and then re-sampled to 256 Hz. Finally, the EOG signals are segmented into one-dimensional segments of 2 s.

For the myogenic artifact segments (figure 1(c)), a facial EMG dataset is used [59]. We choose facial EMG because they are the main sources of myogenic artifacts. The raw EMG signal is band-pass filtered

Table 1. Summary of the data collections used in our dataset.

Dataset	Signal type	# of subjects	Mean age \pm SD	Dataset website
Hohyun <i>et al</i> (2017) [53]	EEG	52	26 \pm 3.86	http://gigadb.org/dataset/100295
Kangoga <i>et al</i> (2016) [54]	EOG	20	22.75 \pm 1.45	http://u4ag2kanosr1.blogspot.jp/
Naem <i>et al</i> [56]	EOG	8	23.8 \pm 2.5	www.bbci.de/competition/iv/
Schlögl <i>et al</i> (2007) [57, 58]	EOG	10	Age between 17 and 31	www.bbci.de/competition/iv/
Rantanen <i>et al</i> (2015) [59]	EMG	15	40.7 \pm 9.6	https://etsin.fairdata.fi/dataset/0f24bf09-c5d1-422e-8df5-eb44219f5dec



between 1 and 120 Hz and notched at the powerline frequency, and then resampled to 512 Hz. We resample the EMG to 512 Hz instead of 256 Hz, because the EMG signal is concentrated in the high frequency range, so a higher sampling rate is required (according to the Nyquist sampling theorem). In the end, we extract one-dimensional 2 s EMG segments.

For all three categories, the segments are standardized by subtracting their mean and dividing by their standard deviation, and then visually inspected by an expert. We obtain a total of 4514 EEG segments, 3400 ocular artifact segments, and 5598 myogenic artifact segments. The segments of each category are respectively saved as Matlab matrix files and

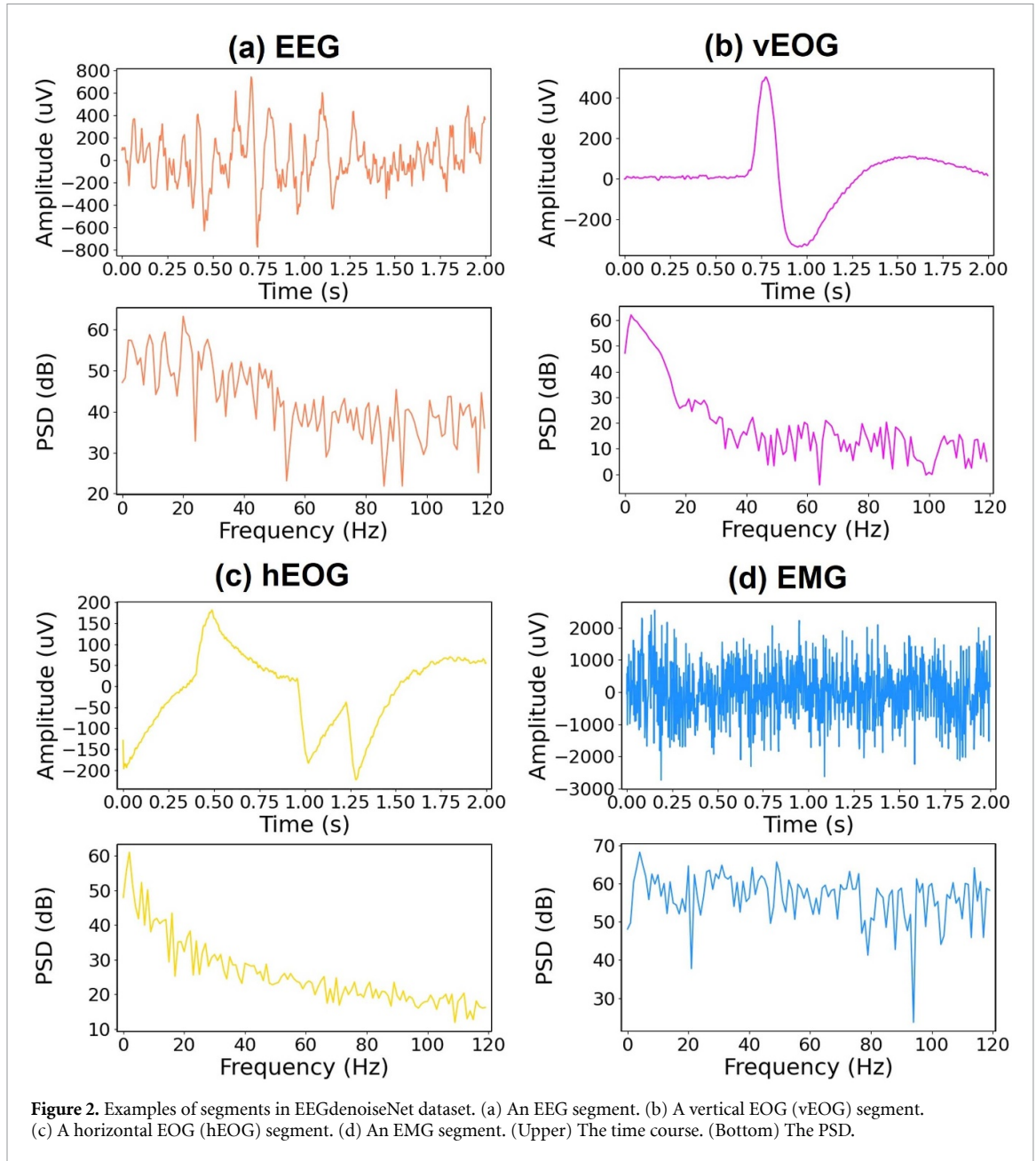


Figure 2. Examples of segments in EEGdenoiseNet dataset. (a) An EEG segment. (b) A vertical EOG (vEOG) segment. (c) A horizontal EOG (hEOG) segment. (d) An EMG segment. (Upper) The time course. (Bottom) The PSD.

Python numpy matrix files in the public data repository. Figure 2 shows an example of the clean EEG, horizontal EOG, vertical EOG and EMG.

2.2. Data usage

The contaminated signals can be generated by linearly mixing the pure EEG segments with EOG or EMG artifact segments, according to equation (1) (see figure 1(c)):

$$y = x + \lambda \cdot n, \quad (1)$$

where y denotes the mixed one-dimensional signal of EEG and artifacts; x denotes the clean EEG signal as the ground truth; n denotes (ocular or myogenic) artifacts; λ is a hyperparameter to control the signal-to-noise ratio (SNR) in the contaminated EEG signal y . Specifically, the SNR of the contaminated segment

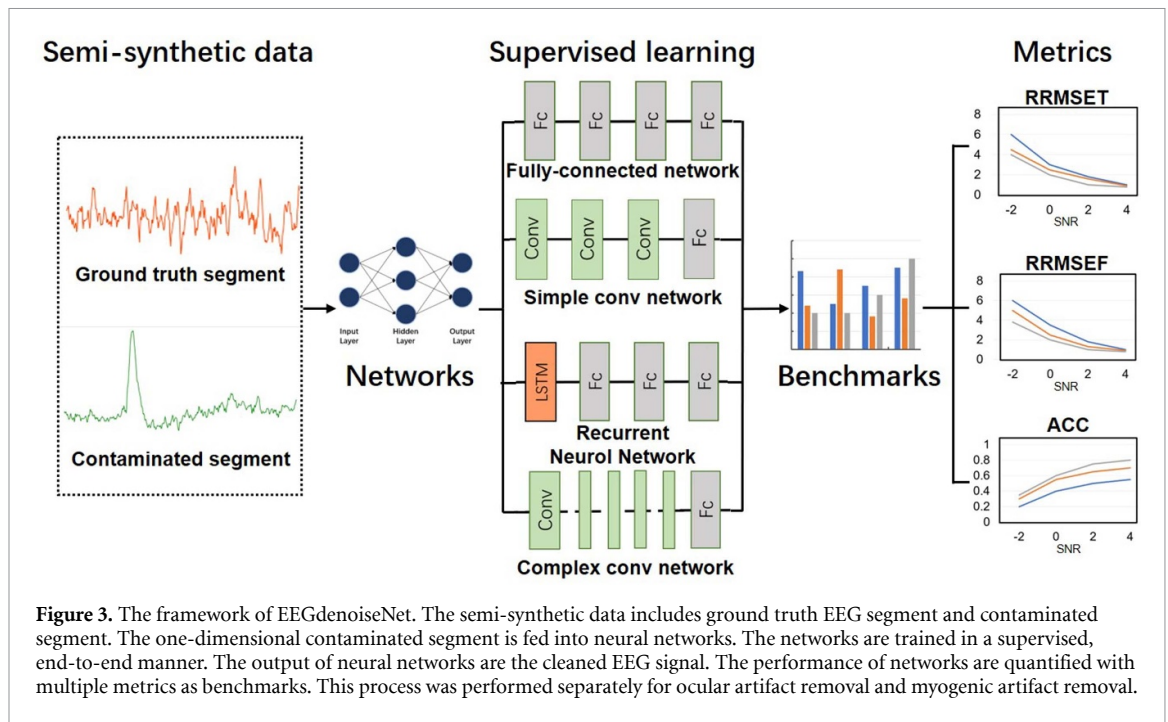
can be adjusted by changing the parameter λ according to equation (2):

$$SNR = 10 \log \frac{RMS(x)}{RMS(\lambda \cdot n)}, \quad (2)$$

in which the root mean squared (RMS) value is defined as equation (3):

$$RMS(g) = \sqrt{\frac{1}{N} \sum_{i=1}^N g_i^2}, \quad (3)$$

where N denotes the number of temporal samples in the segment g , and g_i denotes the i^{th} sample of a segment g . Notably, lower λ represents higher SNR, as less EOG or EMG artifacts are added in the EEG signal. In return, lower SNR means higher noise level. According to previous studies, the SNR of EEG contaminated by ocular artifacts is usually ranging



from -7 to 2 dB [61], while the SNR of EEG contaminated by myogenic artifacts are between -7 and 4 dB [62, 63].

In this way, we obtain a pair of EEG data (x, y) . To train the end-to-end DL methods for EEG denoising, the clean EEG x can be regarded as the ground truth, and the contaminated EEG y can be used as the inputs.

3. Benchmarking deep learning algorithms

The second goal of this study is to provide a set of benchmark algorithms (figure 3). We train four standard deep-learning neural networks, then validate the networks. The evaluation metrics can be used as benchmarks for the EEG denoising algorithms. The neural networks are not trained to classify three types of segments. Instead, we train the benchmarking networks to remove ocular artifacts and myogenic artifacts separately and directly in temporal field.

3.1. Generating semi-synthetic data

The semi-synthetic ocular artifact contaminated signals are from 3400 EEG segments and 3400 ocular artifact segments, with 80% for generating the training set, 10% for generating the validation set, and 10% for generating the test set [64]. Each set were generated by randomly linearly mixing EEG segments and ocular artifact segments according to section 2.2, with SNR raging from ten different SNR levels (-7 , -6 , -5 , -4 , -3 , -2 , -1 , 0 , 1 , 2 dB). This procedure expanded the data size of each set to ten times. The EEG segments are treated as ground truth, and the corresponding mixed segments are treated as contaminated EEG.

The myogenic artifacts contaminated signals come from 4514 EEG segments and 5598 myogenic artifact segments. To match the sampling frequency of EEG segments with myogenic artifact segments, we upsample the EEG segments to 512 Hz. To match the number of EEG segments with myogenic artifact segments, we randomly reuse some EEG segments. We mix the EEG segments and the myogenic artifact segments as equation (1) to generate the training data, test data, and validation data. Likewise, the EEG segments are treated as ground truth, and the corresponding mixed segments are treated as contaminated EEG.

3.2. Network architectures

3.2.1. Fully-connected neural network

A fully-connected network with four hidden layers using ReLu as activation function is provided as a benchmarking algorithm (figure 4(a)). The number of neurons in each layer is equal to the number of temporal samples of the input signal (i.e. 512 for ocular artifact reduction, and 1024 for myogenic artifact reduction). Dropout regularization [65] is used to reduce overfitting. The contaminated EEG is fed in from the first layer of the neural network, and then the denoised EEG is output from the last layer.

3.2.2. Simple convolution neural network

A simple convolution network is implemented (figure 4(b)). The simple CNN consists of four 1D-convolution layers with small 1×3 kernels, 1 stride, and 64 feature maps (k3n64s1). Each 1D-convolution layer is followed by a batch-normalization layer [66] and a ReLu activation function. To reconstruct the signal, the last convolutional layer is followed by a

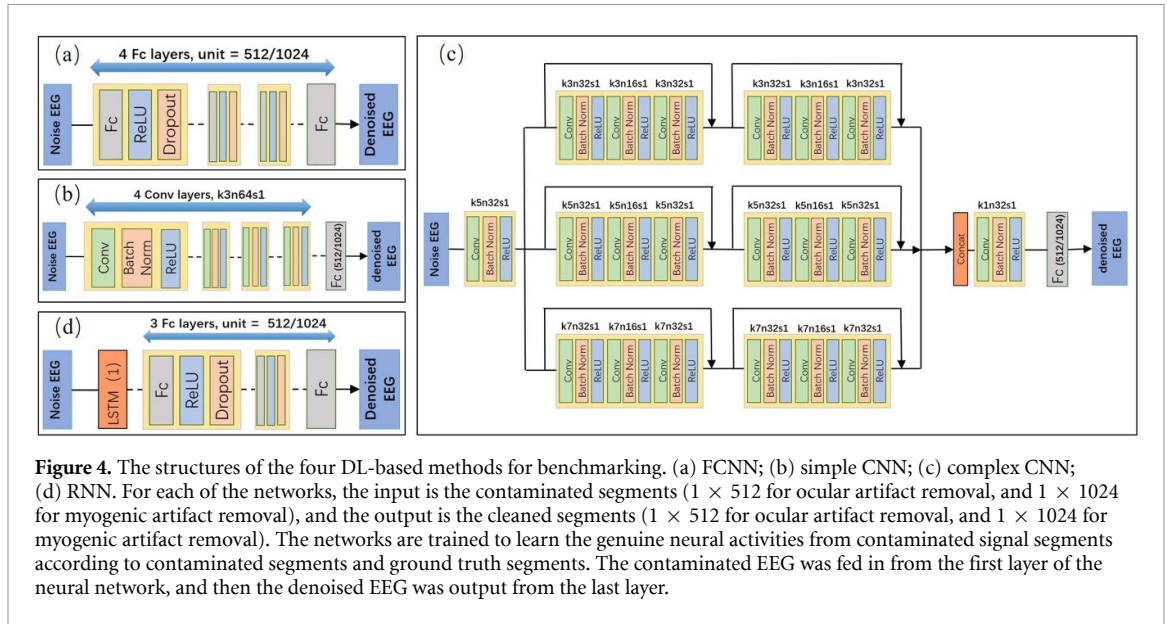


Figure 4. The structures of the four DL-based methods for benchmarking. (a) FCNN; (b) simple CNN; (c) complex CNN; (d) RNN. For each of the networks, the input is the contaminated segments (1×512 for ocular artifact removal, and 1×1024 for myogenic artifact removal), and the output is the cleaned segments (1×512 for ocular artifact removal, and 1×1024 for myogenic artifact removal). The networks are trained to learn the genuine neural activities from contaminated signal segments according to contaminated segments and ground truth segments. The contaminated EEG was fed in from the first layer of the neural network, and then the denoised EEG was output from the last layer.

flatten layer and a dense layer with 512 or 1024 neurons as outputs (the same as the input).

3.2.3. Complex convolution neural network

An one-dimensional residual convolutional neural network (1D-ResCNN), adapted from [38], is implemented (figure 4(c)). Compared with simple CNN, the 1D-ResCNN has a more complex structure, so it is called complex CNN. The main difference between them is that a ResNet with skip-layer connections is added into the complex CNN to avoid gradient explosion so that we can train a deeper network to obtain better feature extraction capabilities [23]. To extract multi-scale features, we repeatedly stack residual blocks, using 1×3 , 1×5 , 1×7 multi-scale convolutional kernels twice and arranging three sets of residual blocks branches in parallel [27, 67].

3.2.4. Recurrent neural network

A long short-term memory (LSTM) network (figure 4(d)), adapted from [68], is regard as the benchmark of RNNs. LSTM can learn long-term dependencies, which may help distinguish the long-term features in noise and EEG signals. Each EEG sample is sequentially input to LSTM cells, and the output is obtained from the state of each cell through a fully-connected network. This RNN model is initialised to have one hidden state, and the output network is a three-layer fully-connected network with ReLU activation function, dropout regularization, and 512 or 1024 neurons per layer.

3.3. Learning process

In order to facilitate the learning procedure, we normalized the input contaminated EEG segment and the ground-truth EEG segment by dividing the standard deviation of contaminated EEG segment according to equation (4):

$$\hat{x} = \frac{x}{\sigma_y}, \quad \hat{y} = \frac{y}{\sigma_y}, \quad (4)$$

where σ_y is the standard deviation of the contaminated EEG signal segment y . The standard deviation of each noise segment is saved, so that the magnitude of the denoised EEG segment can be restored by multiplying the network output by the corresponding standard deviation value.

The networks are trained in an end-to-end manner, which means that we input the normalized contaminated EEG segment into the neural networks and then directly output the denoised EEG segment. To this end, the goal of a denoising network is to learn a nonlinear function f that maps the contaminated EEG \hat{y} to the denoised EEG \tilde{x} :

$$\tilde{x} = f(\hat{y}, \theta), \quad (5)$$

where $\hat{y} \in \mathbb{R}^{1 \times T}$ denotes the contaminated EEG segment, $\tilde{x} \in \mathbb{R}^{1 \times T}$ as the output of neural network (the denoised EEG segment), and the vector θ contains all parameters to be learned.

We use the mean squared error (MSE) as loss function $L_{MSE}(f)$ (see equation (6)). The learning process is implemented with gradient descent to minimize the error between the denoised segment and the ground-truth clean segment:

$$L_{MSE} = \frac{1}{N} \sum_{i=1}^N \left\| \tilde{x}_i - \hat{x}_i \right\|_2^2, \quad (6)$$

where N denotes the number of temporal samples of segment; \tilde{x}_i denotes i th sample of the output of the neural network; \hat{x}_i denotes the i th sample of the ground truth x .

For ocular artifact removal, we train the FCNN with 60 epochs, RNN with 100 epochs, while the simple CNN and complex CNN models are trained

over 40 epochs. For myogenic artifact removal, we train the FCNN and RNN with 60 epochs, while the simple CNN and complex CNN models are trained over 10 epochs. The Adam algorithm is applied to optimize the loss function, and the parameter were set to $\alpha = 5 \times 10^{-5}$, $\beta_1 = 0.5$, $\beta_2 = 0.9$. To increase the statistical power, the four networks are trained, validated and tested independently for 10 times with randomly generated datasets via EEGdenoiseNET.

The time cost of training the network also needs to be considered. It takes about 30 min to train the FCNN and the simple CNN, approximately 1 h to train the complex CNN, and approximately 8 h to train RNN. It should be noted that the time cost largely depends on the software implementation and hardware platform. In our study, the networks were implemented in Python 3.7 with Tensorflow 2.2 library, running on a computer with two NVIDIA Tesla V100 GPUs. The codes for the benchmarking algorithms are publicly available online at Github [69]. The detailed information for network architecture is in the supplementary material (available online at stacks.iop.org/JNE/18/056057/mmedia).

3.4. Performance evaluation as benchmarks

There are several metrics are used to qualitatively evaluate the performance of networks, including the network convergence, the relative root mean squared error (RRMSE), and the correlation coefficient.

The network convergence is the first index to evaluate the performance of networks, which can provide rich information about the learning procedure and generalization ability. The convergence curve of both training and validating processes are obtained by calculating the averaged loss (in equation (6)) with respect to the number of epochs.

We then quantitatively examine the performance of the networks by applying three objective measures to the denoised data [62], including RRMSE in the temporal domain ($RRMSE_{temporal}$, see equation (7)), RRMSE in the spectral domain ($RRMSE_{spectral}$, see equation (8)) and the correlation coefficient (CC see equation (9)):

$$RRMSE_{temporal} = \frac{RMS(f(y) - x)}{RMS(x)}, \quad (7)$$

$$RRMSE_{spectral} = \frac{RMS(PSD(f(y)) - PSD(x))}{RMS(PSD(x))}, \quad (8)$$

where the function $PSD()$ denotes to the power spectral density of an input segment. The frequency range of PSD is 0–120 Hz. The fft-length equal to the length of the input segment:

$$CC = \frac{Cov(f(y), x)}{\sqrt{Var(f(y))Var(x)}}. \quad (9)$$

To compare the DL methods with the traditional methods, we implement two traditional EEG

denoising methods: (a) empirical mode decomposition (EMD) and (b) filtering. In the EMD method, the artifactual intrinsic mode functions are defined by the distance metric used in clustering [70]. In the filtering method, the ocular and myogenic artifacts are removed using a high-pass filter (12 Hz) and a band-pass filter (12–40 Hz), respectively. These two traditional methods are tested 10 times with randomly generated datasets. The corresponding codes are available online at <https://github.com/ncclabsustech/Single-Channel-EEG-Denoise>.

4. Results

To give a qualitative overview of the denoising results, we display some sample fragments in the test in the time domain and frequency domain for ocular artifact removal (see figure 5) and for myogenic artifact removal (see figure 6). For each network and artifact type, we show two examples: one of the best results (left column) and one of the worst result (right column). Generally, both in ocular and myogenic artifact removal, the artefacts are greatly attenuated, and the noise-free EEG samples are well-reconstructed. The frequency domain diagram shows that the artifacts in the low frequency bands are well detected and attenuated, but the high frequency is affected by residual noise.

The quantitatively results are examined. We first present the convergence of the four networks. The training and validation loss of the networks can show a quantitative overview of the training and validating process. For all the four networks and two artifact types, the training loss is consistently lower than the validation loss as expected. For the ocular artifact removal (see figure 7(a)), the training and validation loss decrease with the increase of epochs. Specifically, the loss of simple CNN and complex CNN drop notably fast and eventually diminish after 20 epochs. The FCNN loss and the RNN loss, however, starting from a relatively high level, remain at a significant level after 20 epochs. For the myogenic artifact removal (see figure 7(b)), the training loss of four networks decreased with respect to the number of epochs, similar to the ocular artifact removal. The loss of simple CNN and complex CNN decrease faster during training, but increased during validation. This phenomenon indicates that the two convolutional networks seem not learn the true characteristics of the EMG signal, which means that CNNs suffer from an overfitting problem when removing myogenic artifacts.

We present the quantitative benchmarks ($RRMSE_{temporal}$, $RRMSE_{spectral}$ and CC) from the four networks and the two traditional methods at multiple SNR levels (see figure 8). Generally, for both ocular and myogenic artifact removal, the performance decreases with the decrease of SNR level. The traditional methods showed higher $RRMSE$ and lower

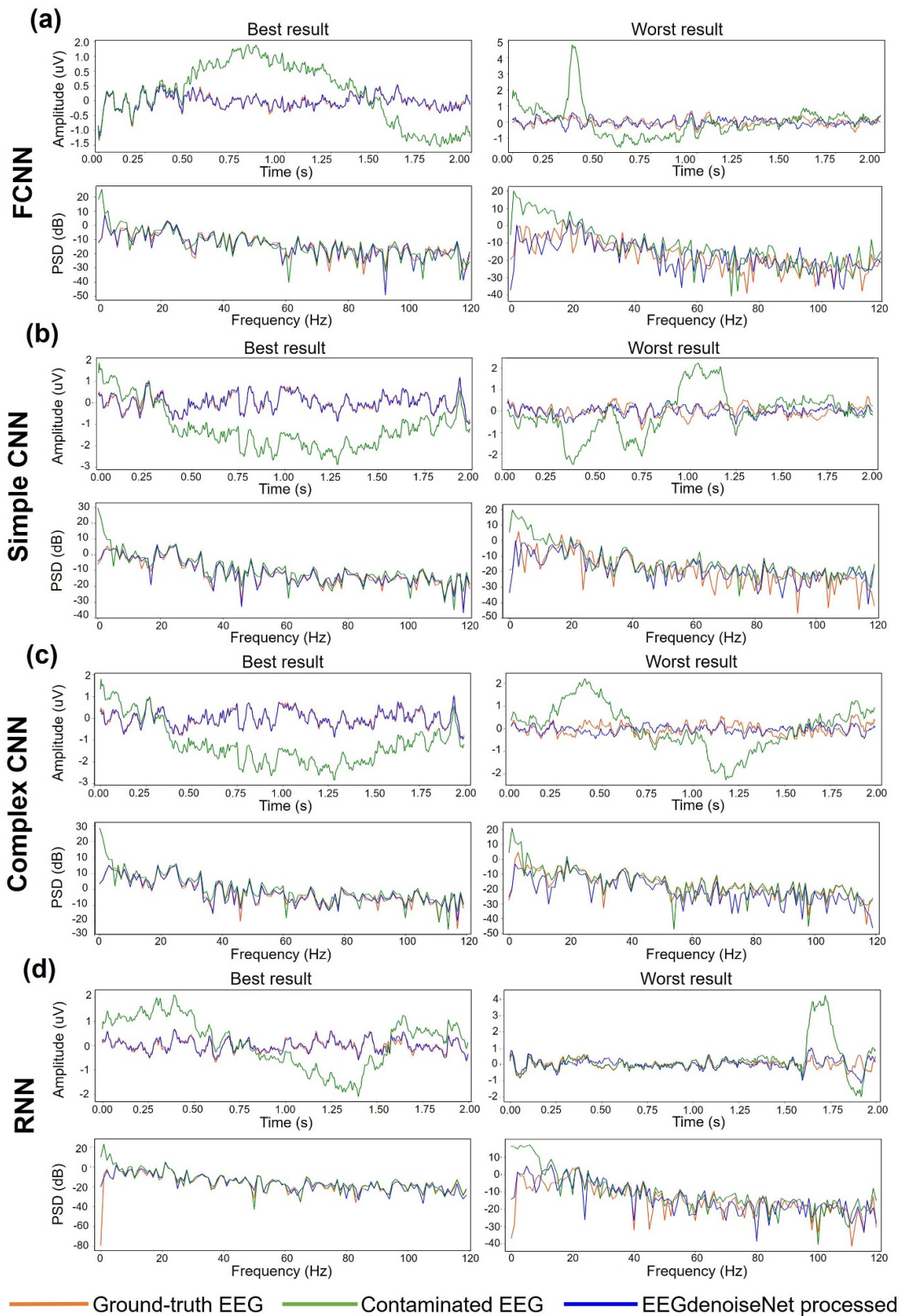


Figure 5. Some exemplary segments of the performance in temporal domain (upper) and spectral domain (bottom) for ocular artifact removal. (a) FCNN. (b) Simple CNN. (c) Complex CNN. (d) RNN. (Left) The examples with the best denoising performance; (right) the examples with the worst denoising performance. The orange, green and blue line are the ground-true EEG, the noisy EEG and the cleaned EEG by EEGdenoiseNet, respectively.

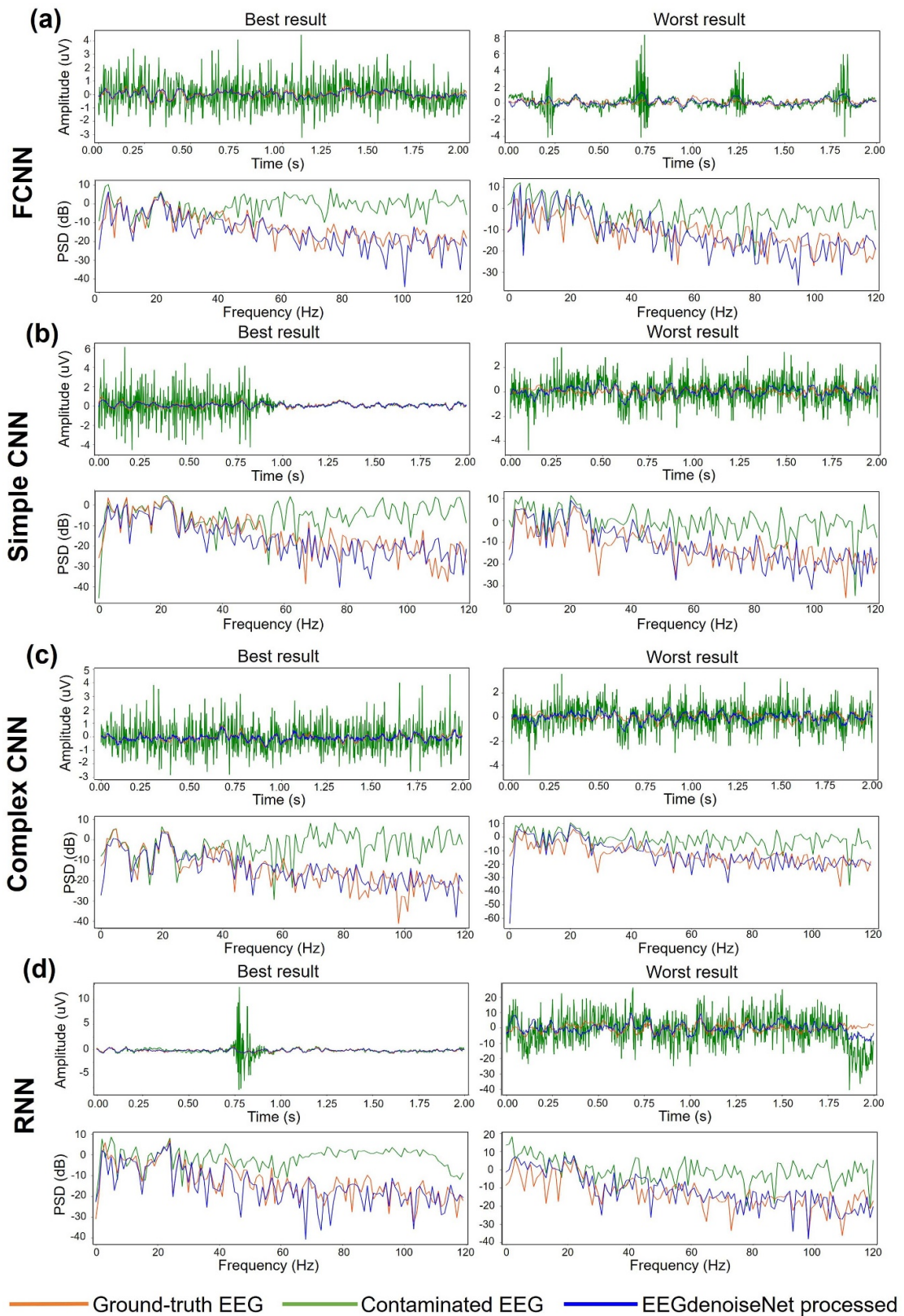
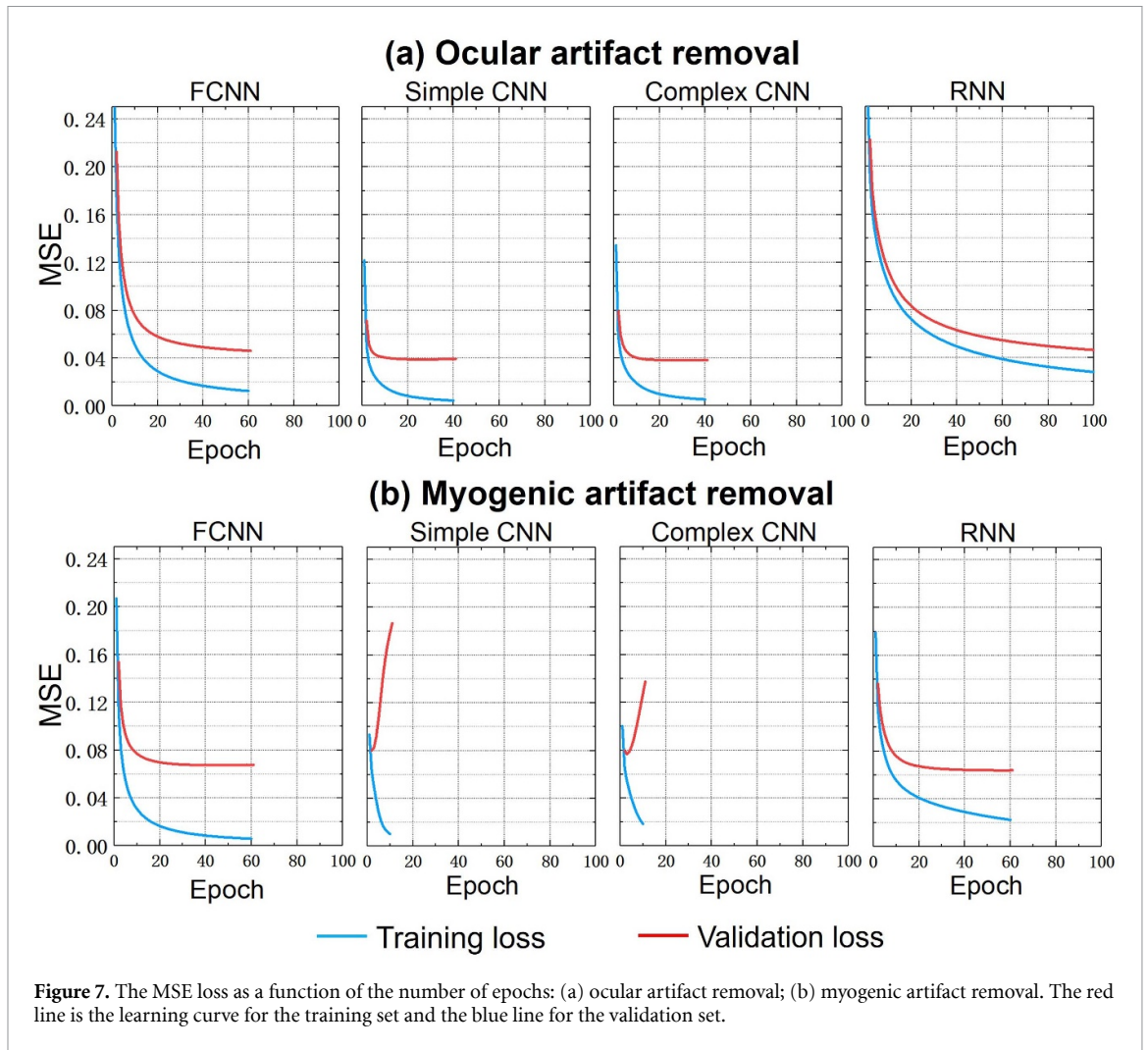


Figure 6. Some exemplary segments showing the performance in temporal (upper) and spectral (bottom) domains for myogenic artifact removal. (a) FCNN. (b) Simple CNN. (c) Complex CNN. (d) RNN. (Left) The examples with the best denoising performance; (right) the examples with the worst denoising performance. The orange, green and blue lines are the ground-true EEG, the noisy EEG and the cleaned EEG by EEGdenoiseNet, respectively.

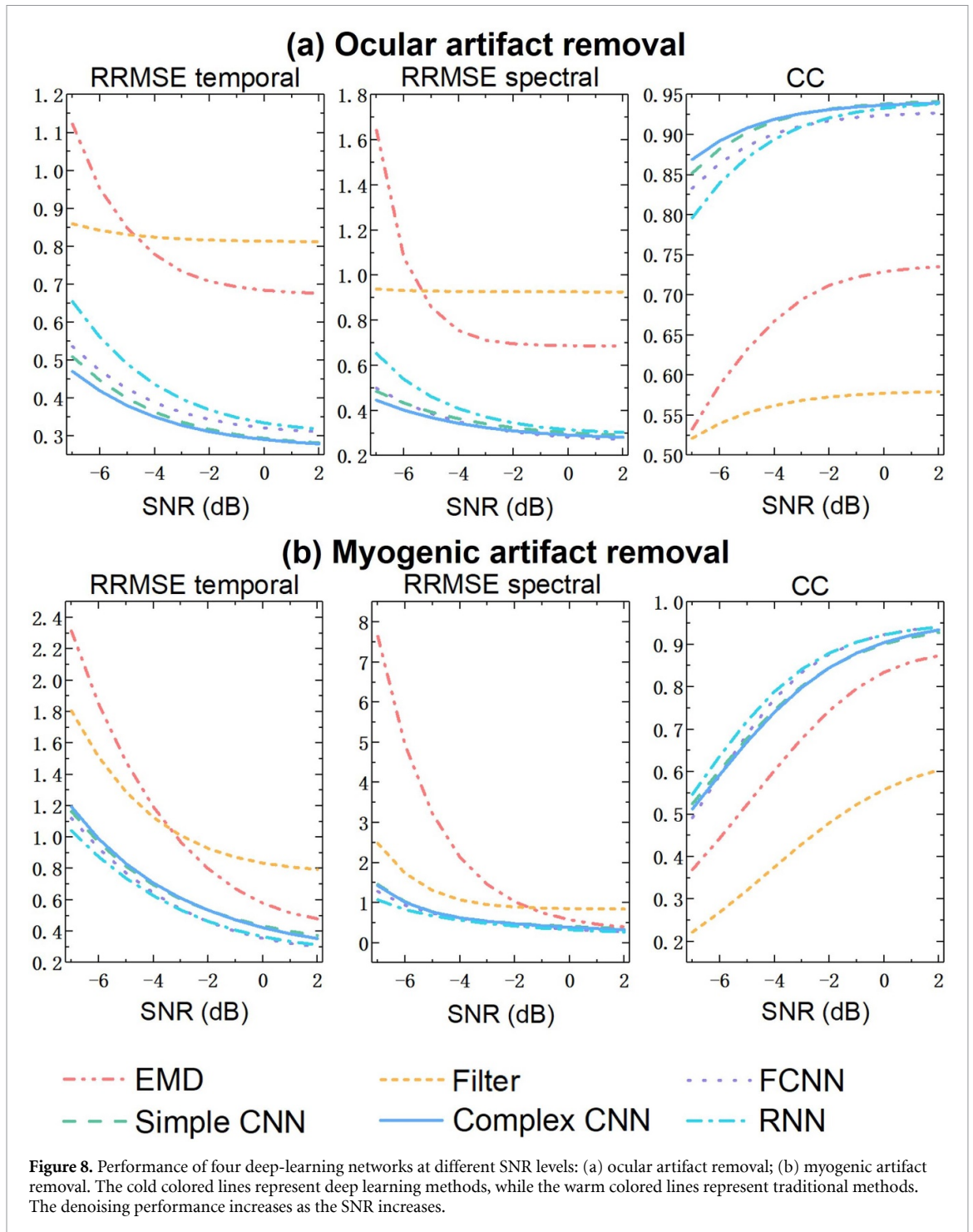


CC compared with the four DL networks. The difference of performance is larger at the large noise level (low SNR), while the difference reduces at low noise level (large SNR, e.g. $SNR > 0$). Among the DL methods, RNN has the lowest $RRMSE$ and the highest CC for ocular artifact removal (see figure 8(a)), and the complex CNN has the lowest $RRMSE$ and the highest CC in myogenic artifact removal.

To further comprehensively compare benchmarks, we separately plot the benchmarks at multiple SNR levels in boxplot (see figure 9), and conduct ANOVA analyses. For the ocular artifact removal (see figure 9(a)), DL-based methods have significantly better denoising performance compared to two traditional methods, in terms of $RRMSE_{temporal}$, $RRMSE_{spectral}$ and CC ($p < 0.001$ for each of three metrics). Similarly, the DL-based methods outperform traditional methods for myogenic artifact removal ($p < 0.001$ for each of three metrics) (see figure 9(b)). In the time domain, $RRMSE_{temporal}$ of RNN is significantly higher than FCNN, simple CNN, and complex CNN ($p = 0.007$, $p < 0.001$, and $p < 0.001$, respectively); FCNN has significantly higher $RRMSE_{temporal}$ than the complex CNN ($p = 0.020$). At the frequency domain, RNN has significantly higher $RRMSE_{spectral}$

than the FCNN and the complex CNN ($p = 0.020$ and $p = 0.006$, respectively). CC of the complex CNN is significantly higher than RNN and FCNN ($p < 0.001$, and $p = 0.011$, respectively). The same effect is shown on simple CNN and RNN ($p = 0.004$).

We finally evaluate the performance of the different methods for different frequency bands, by calculating the average power ratio of each frequency band (delta (1–4 Hz), theta (4–8 Hz), alpha (8–13 Hz), beta (13–30 Hz), and gamma (30–80 Hz) bands) to whole band (1–80 Hz) for ocular artifact removal and myogenic artifact removal (see tables 2 and 3). For the ocular artifact removal (see table 2), the mix of ocular artifacts increased the power ratio of delta and theta bands, while reduced the ratio of the other bands. The simple CNN showed the closest delta, theta and beta power ratio compared to those of the ground truth, the same effect observed on the complex CNN for theta band, on the EMD for alpha band, on the RNN for gamma band, and on the FCNN for theta and gamma band. In myogenic artifact removal (see table 3), the add of myogenic artifact increased gamma power ratio and decreased other power ratios. The FCNN showed the closest ratio in beta bands compared to those of the ground truth, the same



effect on the EMD for alpha band, on the complex CNN for theta and gamma bands, on the RNN for delta and alpha bands.

5. Discussion

In this study, we have provided an EEG benchmark dataset, EEGdenoiseNet, for training and testing end-to-end DL models. To obtain the ground-truth clean EEG data, the raw EEG data is denoised by ICLabel [9] and then manually inspected for a double check. Although there are other publicly available

EEG datasets, they are not specifically developed for EEG denoising. Instead, they are mainly focused on the resting state study [44, 45], psychological study [46–48], or motor imaginary or motor tasks [49–52]. A previous study has offered a semi-simulated dataset for EOG artifact removal, but EMG signals are not included [71]. Effective use of these datasets for DL-based denoising requires extensive EEG background knowledge, including properties of EEG and artifacts, data format conversion, and signal processing. In contrast, the segments in our dataset have been pre-processed, so users can immediately

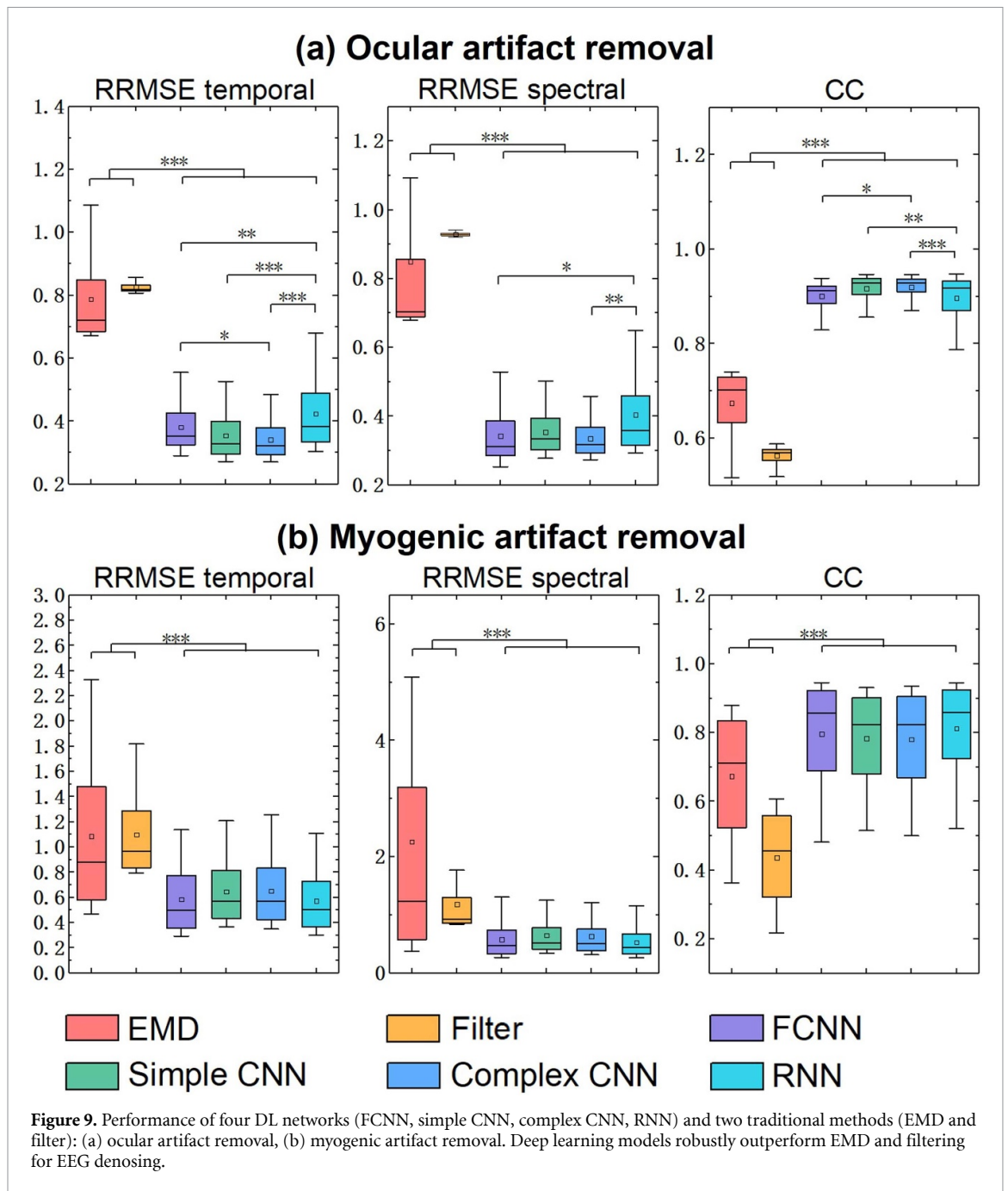


Table 2. Power ratios of different frequency bands before and after ocular artifact removal.

Denosing method	Delta	Theta	Alpha	Beta	Gamma
EMD	0.025	0.042	0.096	0.585	0.252
Filter	0.000	0.000	0.000	0.405	0.595
FCNN	0.129	0.127	0.085	0.500	0.159
Simple CNN	0.131	0.127	0.085	0.492	0.165
Complex CNN	0.128	0.127	0.085	0.493	0.166
RNN	0.124	0.122	0.088	0.506	0.159
Ground truth	0.143	0.141	0.093	0.467	0.157
Contaminated signal	0.514	0.216	0.070	0.151	0.049

'Ground truth' refers to the clean EEG segments.

'Contaminated signal' refers to the mixed EEG signal generated by equation (1).

The highlighted numbers are closest to the value of ground truth.

Abbreviation: EMD, empirical mode decomposition; FCNN, fully-connected neural network; CNN, convolutional neural network; RNN, recurrent neural network.

Table 3. Power ratios of different frequency bands before and after myogenic artifact removal.

Denoising method	Delta	Theta	Alpha	Beta	Gamma
EMD	0.227	0.162	0.093	0.330	0.188
Filter	0.000	0.000	0.000	0.312	0.687
FCNN	0.147	0.144	0.092	0.481	0.135
Simple CNN	0.119	0.138	0.096	0.506	0.142
Complex CNN	0.123	0.139	0.097	0.492	0.149
RNN	0.139	0.138	0.093	0.482	0.147
Ground truth	0.142	0.140	0.093	0.464	0.160
Contaminated signal	0.200	0.141	0.077	0.300	0.281

generate a large set of semi-synthetic noisy EEG segments with ground truth for their DL-based denoising models without being distracted by detailed electrophysiological knowledge. With this advantage, our well-structured dataset would greatly promote the development of DL-based EEG denoising.

Another major challenge to compare the performance of different denoising algorithms is the lack of specific benchmarks. The use of standard benchmarks greatly simplify the comparisons of performance across multiple DL models. To fill this gap, we provided a set of benchmark algorithms along with a standardized EEG dataset. We chose four well-known and relatively basic networks, i.e. a FCNN, a simple CNN, and a RNN for benchmarking. Performance of these DL models in providing artifact-corrected EEG data has been measured using several standard metrics, such as RRMSE, PSD and CC. Furthermore, we define the network convergence, expressed by loss as a function of epoch number, as a qualitative part of the benchmarks. We expect our work to contribute to the DL-based EEG denoising field, in particular for we standardizes evaluation metrics of performance.

Our benchmarks of four DL networks and two traditional methods have demonstrated the feasibility of using DL-based methods to attenuate artifacts from EEG signals. Our comparisons of the four networks (i.e. FCNN, simple CNN, complex CNN, RNN) with two traditional methods (i.e. EMD and filter) suggest that DL-based methods outperform the traditional method, and the supervised end-to-end DL has great potential to remove artifacts in EEG signals. Specifically, for the ocular artifacts, the range of CC values in our four networks are at equivalent level of the CC values reported in a previous study, which used a regression-based method and an offline ICA-based method [72]. A consistent result has been also reported by a DL-based ocular artifact removal study [37]. However, these studies have not offered benchmarks for comparing with other methods [73–76]. For the myogenic artifacts, comparable $RRMSE_{temporal}$ values have been reported in previous literature, such as an ICA-based method [63] and a canonical correlation analysis-based method [77].

The performance of the neural networks depends on the data quality and frequency characteristics of artifacts. The neural networks provide better results

for high SNR signals than low SNR signals (figure 8). Moreover, the high-frequency artifacts, such as EMG artifacts, are more difficult for neural networks to deal with (figures 8 and 9). This phenomenon may be explained by the *F-principle* of neural network [78]. The F-principle proves that DL networks often learn low-frequency information in the early stages of training, and then learn high-frequency information as training iterations increase.

One advantage of DL for EEG artifact removal is its flexibility and generalizability. Although the DL-based denoising methods require a large amount of ground-truth EEG data in the training stage, once the model is trained, it can be easily applied to new data, such as multi-channel EEG data or task-related EEG data, regardless of the corresponding reference channels for artifact removal. Another advantage lies in the handling of complex (e.g. nonlinear and non-stationary) artifact mixtures. Due to the hierarchical structure of deep neural networks, DL models can directly learn the true nature of neural activities from training data in the hidden space, and then generate the cleaned EEG data according to the new contaminated EEG input, whereas traditional methods usually linearly attenuate artifacts. Therefore, methods based on DL are expected to provide better performance than traditional methods in noise removal.

Several limitations should also be mentioned. First of all, an important potential problem is the size of the dataset and the type of data. Although we provided thousands of segments of EEG, ocular and myogenic artifacts in EEGdenoiseNet, it is possible that more complex neural networks might require larger amounts of data for training and testing. Another drawback is the diversity of the EEG type and artifact type. EEG data may be collected in resting state or in different task conditions; furthermore, artifacts in EEG recordings are not only limited to ocular and myogenic. For example, removing motion artifacts is important for EEG mobile applications. To address these drawbacks, better tools for extracting signal segments [79] and criteria for reviewing and approving additional EEG data submissions to EEGdenoiseNet would be needed in future works. Such an evolving dataset will contribute to improve the generalizability of the DL-based EEG denoising networks to diverse brain states. Third, we only focused on the

denoising of 2 s long EEG segments in this study. It is worth noting that some EEG tasks might be longer than 2 s, not to mention the case of resting EEG. In the future, EEGdenoiseNet needs to be extended to adapt to the denoising of continuous EEG. The continuous artifact removal problem can be solved by defining pseudo-segments in continuous EEG recordings, and extracting the hidden relationships between consecutive segments, such that the previous segment can be used in the training stage as input to constrain the denoising process of the current segment. Forth, here we only focus on single-channel EEG denoising, and the DL model learns the temporal information of EEG signals and EOG/EMG artifacts. To use supervised models to learn spatial features, a benchmark data set with multi-channel EEG data must be provided in future. Fifth, the four neural networks in this study serve as benchmarking algorithms for EEGdenoiseNET dataset. Their generalization ability to other kinds of signals are not tested yet. This will be an important future work. Finally, we did not explore unsupervised DL models in this study. When there is no gold standard for clean EEG signals and artifacts, unsupervised DL may be of great importance.

6. Conclusion

In this study, we provided a dataset containing thousands of clean EEG, ocular artifacts and muscular artifact segments, which is suited for benchmarking DL-based EEG denoising methods. The dataset is well-structured and publicly available online in different formats. In addition, we included a set of benchmark tools to facilitate the evaluation of newly developed DL-based EEG denoising models. Our benchmarking results suggested that DL methods have great potential to remove both ocular and myogenic artifacts from EEG data, even at high noise levels. Our study may accelerate the development of DL-based EEG denoising field.

Data availability statement

The data that support the findings of this study are openly available at the following URL/DOI: <https://github.com/ncclabstustech/EEGdenoiseNet>.

Acknowledgments


This work was funded in part by the National Natural Science Foundation of China (62001205), Guangdong Natural Science Foundation Joint Fund (2019A1515111038), Shenzhen Science and Technology Innovation Committee (20200925155957004, KCXFZ2020122117340001, SGDX2020110309280100), Shenzhen Key Laboratory of Smart Healthcare Engineering (ZDSYS20200811144003009).

Conflict of interest

The authors declare no competing interests.

ORCID iDs


Haoming Zhang  <https://orcid.org/0000-0002-0756-2407>

Mingqi Zhao  <https://orcid.org/0000-0002-2804-9565>

Chen Wei  <https://orcid.org/0000-0003-2999-2771>

Dante Mantini  <https://orcid.org/0000-0001-6485-5559>

Zherui Li  <https://orcid.org/0000-0001-7992-9995>

Quanying Liu  <https://orcid.org/0000-0002-2501-7656>

References

- [1] Cai H, Qu Z, Li Z, Zhang Y, Hu X and Hu B 2020 Feature-level fusion approaches based on multimodal EEG data for depression recognition *Inf. Fusion* **59** 127–38
- [2] Oberman L M, Hubbard E M, Mcclery J P, Altschuler E L, Ramachandran V S and Pineda J A 2005 EEG evidence for mirror neuron dysfunction in autism spectrum disorders *Cogn. Brain Res.* **24** 190–8
- [3] Wolpaw J R, Mcfarland D J, Neat G W and Forneris C 1991 An EEG-based brain-computer interface for cursor control *Electroencephalogr. Clin. Neurophysiol.* **78** 252–9
- [4] Herrmann C and Demiralp T 2005 Human EEG gamma oscillations in neuropsychiatric disorders *Clin. Neurophysiol.* **116** 2719–33
- [5] Liu Q, Farahibozorg S, Porcaro C, Wenderoth N and Mantini D 2017 Detecting large-scale networks in the human brain using high-density electroencephalography *Hum. Brain Mapp.* **38** 4631–43
- [6] Zhao M, Marino M, Samogin J, Swinnen S P and Mantini D 2019 Hand, foot and lip representations in primary sensorimotor cortex: a high-density electroencephalography study *Sci. Rep.* **9** 1–12
- [7] Croft R J and Barry R J 2000 Removal of ocular artifact from the EEG: a review *Clin. Neurophysiol.* **30** 5–19
- [8] Muthukumaraswamy S D 2013 High-frequency brain activity and muscle artifacts in MEG/EEG: a review and recommendations *Front. Hum. Neurosci.* **7** 138
- [9] Piontonachini L, Kreutzdelgado K and Makeig S 2019 ICLabel: an automated electroencephalographic independent component classifier, dataset and website *Neuroimage* **198** 181–97
- [10] Cohen M X 2014 *Analyzing Neural Time Series Data: Theory and Practice* (Cambridge, MA: MIT Press)
- [11] Chaumon M, Bishop D V M and Busch N A 2015 A practical guide to the selection of independent components of the electroencephalogram for artifact correction *J. Neurosci. Methods* **250** 47–63
- [12] Mcmenamin B W, Shackman A J, Maxwell J S, Bachhuber D R W, Koppenhaver A M, Greischar L L and Davidson R J 2010 Validation of ICA-based myogenic artifact correction for scalp and source-localized EEG *Neuroimage* **49** 2416–32
- [13] Gratton G, Coles M G H and Donchin E 1983 A new method for off-line removal of ocular artifact *Electroencephalogr. Clin. Neurophysiol.* **55** 468–84
- [14] Croft R J and Barry R J 2000 EOG correction: which regression should we use? *Psychophysiology* **37** 123–5
- [15] McMenamin B W, Shackman A J, Maxwell J S, Greischar L L and Davidson R J 2009 Validation of regression-based myogenic correction techniques for scalp and source-localized EEG *Psychophysiology* **46** 578–92

- [16] He P, Wilson G and Russell C 2004 Removal of ocular artifacts from electro-encephalogram by adaptive filtering *Med. Biol. Eng. Comput.* **42** 407–12
- [17] He P, Wilson G, Russell C and Gerschütz M 2007 Removal of ocular artifacts from the EEG: a comparison between time-domain regression method and adaptive filtering method using simulated data *Med. Biol. Eng. Comput.* **45** 495–503
- [18] Wold S, Esbensen K and Geladi P 1987 Principal component analysis *Chemometr. Intell. Lab. Syst.* **2** 37–52
- [19] Hyvärinen A and Oja E 2000 Independent component analysis: algorithms and applications *Neural Netw.* **13** 411–30
- [20] Chen X, Xu X, Liu A, Lee S, Chen X, Zhang X, McKeown M J and Wang Z J 2019 Removal of muscle artifacts from the EEG: a review and recommendations *IEEE Sens. J.* **19** 5353–68
- [21] Jung T-P, Makeig S, Westerfield M, Townsend J, Courchesne E and Sejnowski T J 2000 Removal of eye activity artifacts from visual event-related potentials in normal and clinical subjects *Clin. Neurophysiol.* **111** 1745–58
- [22] Krizhevsky A, Sutskever I and Hinton G E 2012 Imagenet classification with deep convolutional neural networks *Advances in Neural Information Processing Systems* pp 1097–105
- [23] He K, Zhang X, Ren S and Sun J 2016 Deep residual learning for image recognition *Proc. IEEE Conf. Computer Vision and Pattern Recognition* pp 770–8
- [24] Mikolov T, Chen K, Corrado G and Dean J 2013 Efficient estimation of word representations in vector space (arXiv:1301.3781)
- [25] Vaswani A, Shazeer N, Parmar N, Uszkoreit J, Jones L, Gomez A N, Kaiser Ł and Polosukhin I 2017 Attention is all you need *Advances in Neural Information Processing Systems* pp 5998–6008 (arXiv:1706.03762)
- [26] Simonyan K and Zisserman A 2014 Very deep convolutional networks for large-scale image recognition (arXiv:1409.1556)
- [27] Szegedy C, Vanhoucke V, Ioffe S, Shlens J and Wojna Z 2016 Rethinking the inception architecture for computer vision *Proc. IEEE Conf. Computer Vision and Pattern Recognition* pp 2818–26
- [28] Sutskever I, Vinyals O and Le Q V 2014 Sequence to sequence learning with neural networks *Advances in Neural Information Processing Systems* pp 3104–12 (arXiv:1409.3215)
- [29] Roy Y, Banville H, Albuquerque I, Gramfort A, Falk T H and Faubert J 2019 Deep learning-based electroencephalography analysis: a systematic review *J. Neural Eng.* **16** 051001
- [30] Sakhavi S, Guan C and Yan S 2015 Parallel convolutional-linear neural network for motor imagery classification European Signal Processing Conf. 2736–4
- [31] Tabar Y R and Halici U 2017 A novel deep learning approach for classification of EEG motor imagery signals *J. Neural Eng.* **14** 016003
- [32] Tang Z, Li C and Sun S 2017 Single-trial EEG classification of motor imagery using deep convolutional neural networks *Optik* **130** 11–18
- [33] Luo T-J, Fan Y, Chen L, Guo G and Zhou C 2020 EEG signal reconstruction using a generative adversarial network with Wasserstein distance and temporal-spatial-frequency loss *Front. Neuroinform.* **14** 15
- [34] Corley I A and Huang Y 2018 Deep EEG super-resolution: upsampling EEG spatial resolution with generative adversarial networks 2018 IEEE EMBS Int. Conf. Biomedical & Health Informatics (BHI) 100–3
- [35] Hartmann K, Schirrmester R and Ball T 2018 EEG-GAN: generative adversarial networks for electroencephalographic (EEG) brain signals (arXiv:1806.01875)
- [36] Fahimi F, Dosen S, Ang K K, Mrachacz-Kersting N and Guan C 2020 Generative adversarial networks-based data augmentation for brain-computer interface *IEEE Trans. Neural Netw. Learn. Syst.* **32** 4039–51
- [37] Yang B, Duan K, Fan C, Hu C and Wang J 2018 Automatic ocular artifacts removal in EEG using deep learning *Biomed. Signal Process. Control* **43** 148–58
- [38] Sun W, Su Y, Wu X and Wu X 2020 A novel end-to-end 1D-ResCNN model to remove artifact from EEG signals *Neurocomputing* **404** 108–21
- [39] Hanrahan C 2019 Noise reduction in EEG signals using convolutional autoencoding techniques Masters University of Dublin (<https://arrow.tudublin.ie/scschcomdis/188/>)
- [40] Zhang H, Wei C, Zhao M, Wu H and Liu Q 2020 A novel convolutional neural network model to remove muscle artifacts from EEG *IEEE Int. Conf. on Acoustics, Speech and Signal Processing (ICASSP)* 1265–9
- [41] Deng J, Dong W, Socher R, Li Li-J, Li K and Fei-Fei Li 2009 ImageNet: a large-scale hierarchical image database 2009 *IEEE Conf. Computer Vision and Pattern Recognition (IEEE)* pp 248–55
- [42] Defferrard M, Benzi K, Vandergheynst P and Bresson X 2016 FMA: a dataset for music analysis (arXiv:1612.01840)
- [43] Panchenko A, Ruppert E, Faralli S, Ponsetto S P and Biemann C 2017 Building a web-scale dependency-parsed corpus from CommonCrawl (arXiv:1710.01779)
- [44] Trujillo L T, Stanfield C T and Vela R D 2017 The effect of electroencephalogram (EEG) reference choice on information-theoretic measures of the complexity and integration of EEG signals *Front. Neurosci.* **11** 425
- [45] Torkamani-Azar M, Kanik S D, Aydin S and Cetin M 2020 Prediction of reaction time and vigilance variability from spatio-spectral features of resting-state EEG in a long sustained attention task *IEEE J. Biomed. Health Inform.* **24** 2550–8
- [46] Koelstra S, Muhl C, Soleymani M, Lee J-S, Yazdani A, Ebrahimi T, Pun T, Nijholt A and Patras I 2011 DEAP: a database for emotion analysis; using physiological signals *IEEE Trans. Affective Comput.* **3** 18–31
- [47] Van Veen G, Barachant A, Andreev A, Cattan G, Rodrigues P C and Congedo M 2019 Building brain invaders: EEG data of an experimental validation (arXiv:1905.05182)
- [48] Korczowski L, Cederhout M, Andreev A, Cattan G, Rodrigues P C, Gautheret V and Congedo M 2019 Brain invaders calibration-less P300-based BCI with modulation of flash duration dataset (bi2015a) *Arch. Ouvertes* **1** 140047
- [49] Luciw M D, Jarocka E and Edin B B 2014 Multi-channel EEG recordings during 3,936 grasp and lift trials with varying weight and friction *Sci. Data* **1** 140047
- [50] Schirrmester R T, Springenberg J T, Fiederer L D J, Glasstetter M, Eggensperger K, Tangermann M, Hutter F, Burgard W and Ball T 2017 Deep learning with convolutional neural networks for EEG decoding and visualization *Hum. Brain Mapp.* **38** 5391–420
- [51] Schalk G, McFarland D J, Hinterberger T, Birbaumer N and Wolpaw J R 2004 BCI2000: a general-purpose brain-computer interface (BCI) system *IEEE Trans. Biomed. Eng.* **51** 1034–43
- [52] Kaya M, Binli M K, Ozbay E, Yanar H and Mishchenko Y 2018 A large electroencephalographic motor imagery dataset for electroencephalographic brain computer interfaces *Sci. Data* **5** 180211
- [53] Hohyun C, Minkyu A, Sangtae A, Moonyoung K and Chan J S 2017 EEG datasets for motor imagery brain computer interface *Gigaence* **6** gix034
- [54] Kanoga S, Nakanishi M and Mitsukura Y 2016 Assessing the effects of voluntary and involuntary eyeblinks in independent components of electroencephalogram *Neurocomputing* **193** 20–32
- [55] Fatourech M, Bashashati A, Ward R K and Birch G E 2007 EMG and EOG artifacts in brain computer interface systems: a survey *Clin. Neurophysiol.* **118** 480–94
- [56] Naem M, Brunner C, Leeb R, Graimann B and Pfurtscheller G 2006 Separability of four-class motor

- imagery data using independent components analysis *J. Neural Eng.* **3** 208–16
- [57] Schlögl A, Keinrath C, Zimmermann D, Scherer R, Leeb R and Pfurtscheller G 2007 A fully automated correction method of eog artifacts in EEG recordings *Clin. Neurophysiol.* **118** 98–104
- [58] Schlögl A, Kronegg J, Huggins J and Mason S 2007 Evaluation criteria for BCI research *Toward Brain-Computer Interfacing* (Cambridge, MA: MIT Press)
- [59] Rantanen V, Ilves M, Vehkaoja A, Kontunen A, Lylykangas J, Mäkelä E, Rautiainen M, Surakka V and Lekkala J 2016 A survey on the feasibility of surface EMG in facial pacing *2016 38th Annual Int. Conf. IEEE Engineering in Medicine and Biology Society (EMBC) vol 2016* pp 1688–91
- [60] Brunner C, Naem M, Leeb R, Graimann B and Pfurtscheller G 2007 Spatial filtering and selection of optimized components in four class motor imagery EEG data using independent components analysis *Pattern Recognit. Lett.* **28** 957–64
- [61] Wang G, Teng C, Li K, Zhang Z and Yan X 2016 The removal of EOG artifacts from EEG signals using independent component analysis and multivariate empirical mode decomposition *IEEE J. Biomed. Health Inform.* **20** 1301–8
- [62] Chen X, Peng H, Yu F and Wang K 2017 Independent vector analysis applied to remove muscle artifacts in EEG data *IEEE Trans. Instrum. Meas.* **66** 1770–9
- [63] De Clercq W, Vergult A, Vanrumste B, Van Paesschen W and Van Huffel S 2006 Canonical correlation analysis applied to remove muscle artifacts from the electroencephalogram *IEEE Trans. Biomed. Eng.* **53** 2583–7
- [64] Kohavi R 1995 A study of cross-validation and bootstrap for accuracy estimation and model selection *Int. Joint Conf. Artificial Intelligence* (<https://dl.acm.org/doi/10.5555/1643031.1643047>)
- [65] Hinton G E, Srivastava N, Krizhevsky A, Sutskever I and Salakhutdinov R R 2012 Improving neural networks by preventing co-adaptation of feature detectors (arXiv:1207.0580)
- [66] Ioffe S and Szegedy C 2015 Batch normalization: accelerating deep network training by reducing internal covariate shift (arXiv:1502.03167)
- [67] Zagoruyko S and Komodakis N 2016 Wide residual networks (arXiv:1605.07146)
- [68] Hochreiter S and Schmidhuber J 1997 Long short-term memory *Neural Comput.* **9** 1735–80
- [69] Zhang H, Zhao M, Wei C, Mantini D, Li Z and Liu Q *EEGdenoiseNet* (Available at: <https://github.com/nclabstustech/EEGdenoiseNet>)
- [70] Mert A and Akan A 2014 Hilbert–Huang transform based hierarchical clustering for EEG denoising *21st European Signal Processing Conf. (EUSIPCO 2013) 1–5* (<https://ieeexplore.ieee.org/document/6811449>)
- [71] Klados M A and Bamidis P D 2016 A semi-simulated EEG/EOG dataset for the comparison of EOG artifact rejection techniques *Data Brief* **8** 1004–6
- [72] Guarnieri R, Marino M, Barban F, Ganzetti M and Mantini D 2018 Online EEG artifact removal for BCI applications by adaptive spatial filtering *J. Neural Eng.* **15** 056009
- [73] Nguyen H-A T et al 2012 EOG artifact removal using a wavelet neural network *Neurocomputing* **97** 374–89
- [74] Woestenburg J C, Verbaten M N and Slangen J L 1983 The removal of the eye-movement artifact from the EEG by regression analysis in the frequency domain *Biol. Psychol.* **16** 127–47
- [75] Elbert T, Lutzenberger W, Rockstroh B and Birbaumer N 1985 Removal of ocular artifacts from the EEG—a biophysical approach to the EOG *Electroencephalogr. Clin. Neurophysiol.* **60** 455–63
- [76] Gómez-Herrero G, De Clercq W, Anwar H, Kara O, Egiazarian K, Van Huffel S and Van Paesschen W 2006 Automatic removal of ocular artifacts in the EEG without an EOG reference channel *Proc. 7th Nordic Signal Processing Symp.—NORSIG 2006 (IEEE)* pp 130–3
- [77] Chen X, Peng H, Yu F and Wang K 2017 Independent vector analysis applied to remove muscle artifacts in EEG data *IEEE Trans. Instrum. Meas.* **66** 1770–9
- [78] John Xu Z-Q, Zhang Y, Luo T, Xiao Y and Ma Z 2019 Frequency principle: Fourier analysis sheds light on deep neural networks (arXiv:1901.06523)
- [79] Mahmoodi M, Makkiabadi B, Mahmoudi M and Sanei S 2021 A new method for accurate detection of movement intention from single channel EEG for online BCI *Comput. Methods Programs Biomed.* **1** 100027